Rapid Communications | Editors' Suggestion

Reducing intrinsic energy dissipation in diamond-on-diamond mechanical resonators toward one million quality factor

Haihua Wu,[1,2] Liwen Sang,[1] Yumeng Li,[1,3] Tokuyuki Teraji,[1] Tiefu Li,[4,*] Masataka Imura,[1] Jianqiang You,[2] Yasuo Koide,[1] Masaya Toda,[5] and Meiyong Liao[1,†]

[1]*National Institute for Materials Sciences, Namiki 1-1, Tsukuba, Ibaraki 305-0044, Japan*
[2]*Beijing Computational Science Research Center, Beijing 100193, China*
[3]*Department of Chemistry, The College of Wooster, 1189 Beall Avenue, Wooster, Ohio 44691, USA*
[4]*Institute of Microelectronics, Tsinghua University, Beijing 100084, China*
[5]*Graduate School of Engineering, Tohoku University, Sendai 980-8529, Japan*

(Received 5 July 2018; revised manuscript received 21 August 2018; published 28 September 2018)

The reduction of the energy dissipation induced by defects is essential to achieve the ultrahigh-quality-factor mechanical resonators for the applications of quantum platform and high-sensitivity microelectromechanical (MEMS) and nanoelectromechanical system (NEMS) sensors. Single-crystal diamond (SCD) is the ideal material for high-quality-factor mechanical resonators due to its outstanding mechanical properties and intrinsic low-energy dissipation. To achieve mechanical resonators with extreme properties as well as high reliability, it is desirable to develop all-SCD mechanical resonators. By using a smart-cut method and atomic layer etching to remove the defects within the resonators, we achieve the SCD-on-SCD mechanical resonators with ultrahigh quality factors of over one million at room temperature. The quality factors are one or more orders of magnitude higher than those of the state-of-the-art MEMS cantilevers based on polycrystalline diamond, single-crystal silicon, and other crystal materials. The diamond MEMS resonators would be highly promising for sensor application as well as for the scheme for coupling with quantum centers in diamond.

DOI: 10.1103/PhysRevMaterials.2.090601

I. INTRODUCTION

Microelectromechanical system (MEMS) or nanoelectromechanical system (NEMS) resonators have attracted broad interest in sensing, signal processing, and quantum physics [1–5]. One of the bottlenecks in MEMS/NEMS resonators based on the traditional materials such as silicon, oxides, nitrides, or metals is the intrinsic material limitations either in performance or reliability [6,7], due to their intrinsic drawbacks in mechanical, physical, electronic, and chemical properties. The quality (Q) factor, a key figure of merit of the MEMS/NEMS resonator, determines the device performance, for example, the minimum detectable force in a MEMS/NEMS sensor [8] and the coupling strength of the resonator with quantum centers [4]. Diamond has the best figures of merits for next-generation MEMS/NEMS to boost the performance and reliability due to its outstanding mechanical, electronic, and thermal properties [9–12]. Compared to other materials, diamond shows the lowest intrinsic energy mechanical loss to achieve an ultrahigh Q factor. Polycrystalline diamonds (PCDs) have been widely investigated for MEMS/NEMS applications and great progress has been achieved [13–18]. However, the grain boundaries and sp^2 content in PCDs limit the ultimate performance and reliability of MEMS/NEMS. To achieve a MEMS/NEMS resonator with an ultrahigh Q factor, single-crystal diamond (SCD) is desirable. Due to the mechanical hardness and chemical inertness of diamond, a deep etching method as done in single-crystal silicon MEMS has not been established yet. Recently, encouraging results were achieved on SCD mechanical resonators by using a diamond-on-insulator (DOI) method [10,11]. Generally, bonding diamond to a foreign substrate has the problem of the difference in thermal expansion coefficients between diamond and the substrate in the DOI method. Moreover, the application of the SCD MEMS/NEMS bonded to a foreign substrate under high temperatures may encounter poor reliability. To achieve high-performance and high-reliability MEMS/NEMS, it is desirable to develop all diamond MEMS/NEMS compatible with the diamond electronics for integration.

In this work, we demonstrate ultrahigh Q factors and highly reliable SCD-on-SCD mechanical resonators fabricated by using a smart-cut method. In the smart-cut method, an ion beam with high energy larger than 100 keV [19] is impinged on the SCD substrate and induces phase transition within the diamond as the sacrificial layer. An atomic layer etching (ALE) combining with a controllable high-quality diamond growth technique is adopted to remove the defects within the SCD mechanical resonators with a thickness accuracy less than 1 nm, and, in turn, reduces the intrinsic energy dissipation in the resonators. As a result, all-SCD nature MEMS resonators with ultrahigh Q factors over 1 000 000 are achieved. The Q factor is superior to those of the state-of-the-art MEMS cantilevers based on PCDs, single-crystal silicon, and other crystal materials [7,19,20].

*litf@tsinghua.edu.cn
†meiyong.liao@nims.go.jp

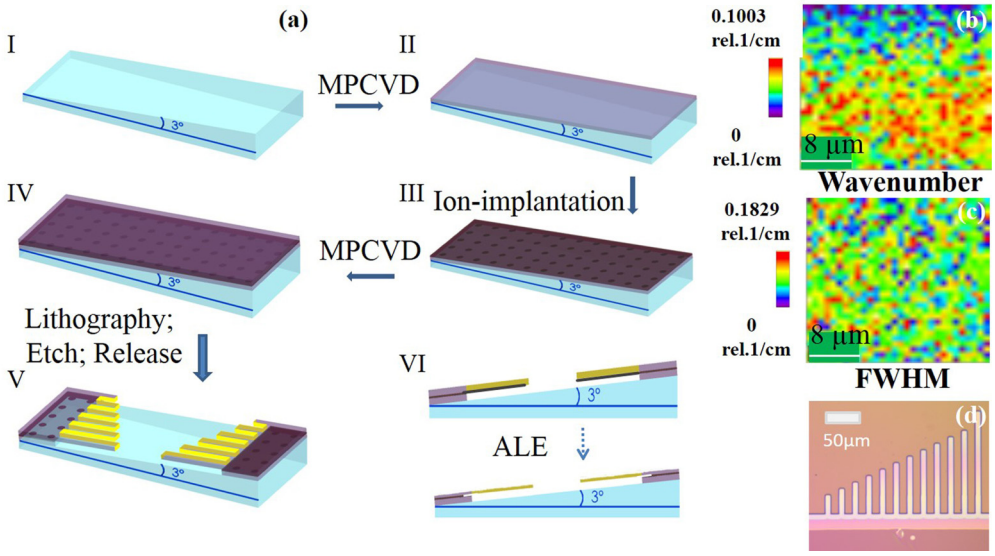

FIG. 1. (a) The schematic diagram of the fabrication process of SCD cantilevers. The fabrication started from (I) a high-pressure, high-temperature (HPHT) type-Ib SCD (100) substrate with 3° off angle; (II) a 10-μm SCD layer about growth by MPCVD. (III) ion implantation; (IV) a second diamond layer (1.6 μm) growth; (V) photolithography, etching, and release of the SCD cantilevers; (VI) ALE etching. The 2D Raman mappings of the homoepitaxial diamond film with spatial distribution of (b) wave number and (c) FWHM. The color bar showing the variation of wave number with reference of 1332 cm^{-1} and FWHM with reference of 2.8 cm^{-1}. (d) Optical image of the SCD cantilevers after the ALE treatment. Dotlike structure: implanted region in diamond.

II. EXPERIMENT

The fabrication of the SCD cantilevers was based on the ion-implantation induced phase transition (IPT) within diamond, which was previously used for the fabrication of freestanding SCD structures and NEMS switches [19,21–25]. The fabrication schematic of our SCD cantilevers is depicted in Fig. 1(a). The process includes (i) a first 10-μm-thick SCD layer growth on a high-pressure, high-temperature (HPHT) type-Ib SCD (100) substrate with a 3° off angle to obtain a high-quality diamond epilayer with a flat surface [26] by a microwave plasma chemical vapor deposition (MPCVD) apparatus [27–31]; (ii) carbon ion implantation at an energy of 180 keV, a dose of 10^{16} cm^{-2}, and an off angle of 7°, (iii) a second growth of 1.6-μm-thick diamond layer; and (iv) release of the SCD cantilevers. The SCD cantilevers contain basically two SCD layers: the second homoepitaxial layer and the bottom ion damaged epitaxial layer, as illustrated in Fig. 1(a) (I–VI). During the MPCVD growth, a buried graphitelike carbon (GLC) layer was formed in the ion-implanted region. Two-dimensional (2D) Raman spectral mapping (spatial resolution: 2 μm) was used to investigate the crystal quality of the diamond epilayers and cantilevers. The Raman spectrum in Fig. 1(b) reveals the high quality of the SCD epilayers with a full width at half maximum (FWHM) of 2.8 cm^{-1}. The 2D images of the Raman spectra show the good homogeneity of the SCD layer with a wave number/FWHM variation of around 0.1003 and 0.1829 rel.1/cm, respectively, centered at 1332 cm^{-1} [Figs. 1(c) and 1(d)]. To remove the defects within the SCD resonator, ALE treatment was conducted in a vacuum chamber at 500 °C with filled oxygen at a pressure of 0.2 atm for different durations up to 400 h. A H_2 plasma treatment of the cantilevers was further conducted to remove the defects by MPCVD at a temperature of 800 °C, a pressure of 80 Torr, and a H_2 flow rate of 500 SCCM (denotes cubic centimeter per minute at STP).

The resonance frequencies of the SCD resonators were measured through a laser Doppler vibrometer (LDV, LV-1710) in a high-vacuum (10^{-3} Pa) chamber at room temperature. The frequency resolution of the LDV is above 1 Hz. A piezoceramic material was used to actuate the cantilevers by rf signal. The frequency spectra were measured by a lock-in amplifier (LA) with a step of 0.1 Hz or more. The decay times of the SCD cantilevers were obtained by the ring-down method [8,10], in which the vibration amplitudes of the cantilevers at the resonance were recorded by switching on/off the rf signal. Careful attention was paid to exclude the effect of the driving piezoceramic as well as the time constant of the LA.

III. RESULTS AND DISCUSSION

Compared to the DOI method, the IPT method favors the integration of diamond MEMS with diamond electronics [32] operated under harsh environments due to the all-SCD nature. However, it is well known that ion-implantation induced defects severely degraded the Q factors of the resonators at the level of 1000 or less [9,33]. Therefore, it is necessary to remove the ion-implantation damaged layer to achieve ultrahigh-Q-factor SCD resonators. Our approach to reduce the effect of the damages is to grow a high-quality homoepitaxial layer above the ion-implanted layer. Consequently, the defective layer under the homoepitaxial layer is reduced or removed by the ALE method.

In order to understand the details of the structure of the SCD resonators we performed TEM (A JEOL JEM-2100F) and high-resolution TEM (HRTEM) observation on another SCD epilayer grown on the ion-implanted HPHT-SCD substrate. This sample was not released. Therefore, the sandwich

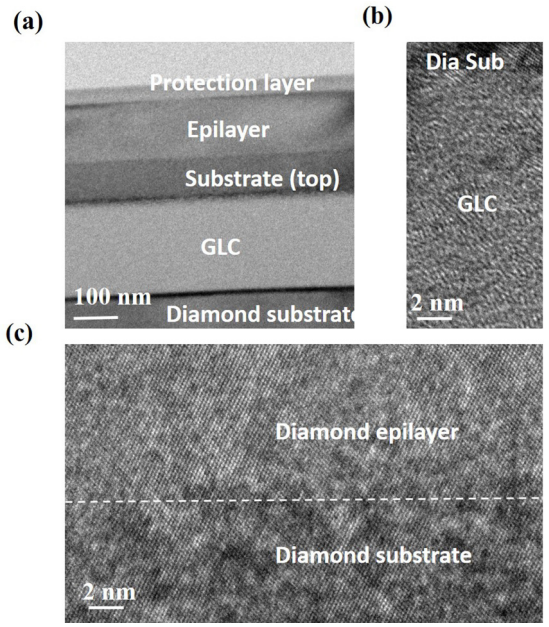

FIG. 2. (a) TEM image revealing the layered structure containing the HPHT SCD substrate (bottom part), buried GLC, SCD substrate (top part), and the SCD epilayer. (b) HRTEM images of (b) the GLC adjacent to the top-part SCD substrate and (c) of the SCD epilayer close to the top-part SCD substrate.

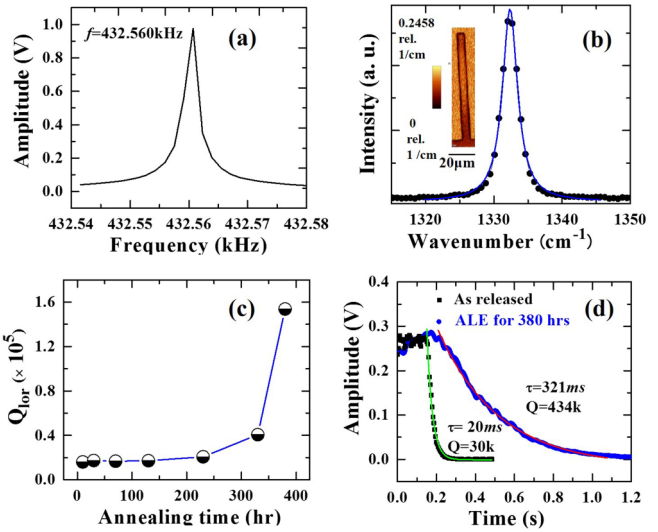

FIG. 3. (a) Resonance frequency spectrum of SCD cantilever S8 with a length of 100 μm and a width of 6 μm. Frequency step: 1.6 Hz, interval time of each step: 3 s. Red line: Lorentzian fitting. (b) Raman spectrum of the SCD cantilever. Inset: 2D Raman mapping throughout the cantilever. (c) Variation of Q factor as ALE duration for cantilever S8. (d) Ring-down measurements of cantilever S8 as released and after ALE for 380 h.

structure of the HPHT SCD substrate containing the bottom-part diamond, GLC, and the top-part diamond can be clearly observed, as shown in Fig. 2(a). The epilayer with different contrast from the top-part diamond of the substrate is also revealed. The thickness of the GLC is around 200 nm and that of the top-part diamond of the substrate is around 100 nm. The GLC nature is disclosed by the HRTEM image shown in Fig. 2(b). The single-crystal nature of the substrate diamond and the adjacent SCD epilayer is realized [Fig. 2(c)]. However, crystalline imperfection is observed at the interface between the GLC and the top-part diamond substrate. Therefore, it is expected that the bottom layer of the SCD cantilever is defective.

We conducted the ALE treatment in an oxygen ambient at 500 °C to reduce/remove the ion-irradiated defects located at the bottom of the cantilevers. The length-dependent resonance frequency of the as-released SCD cantilevers (Fig. S1, Supplemental Material [34]) follows well with the classic Euler-Bernoulli theory as

$$f = k\frac{t}{L^2}\sqrt{\frac{E}{\rho}}, \tag{1}$$

where k is 0.162 for the first resonance mode of a rectangle cantilever; t, L, E, and ρ stand for the thickness, length, Young's modulus, and the mass density of the cantilever, respectively. The Young's modulus of the SCD cantilever was evaluated to be around 1100 GPa. The Q factors of the as-released SCD cantilevers were usually at the level of 10^4 or less (Fig. S2, Supplemental Material [34]). The defective layer due to ion implantation makes a significant contribution to the energy dissipation [35].

The Q factors of the SCD cantilevers are greatly improved by the ALE process. We characterized nearly 100 cantilevers with different dimensions with length from 40 to 160 μm and width from 6 to 10 μm. Figure 3(a) shows a typical resonance frequency spectrum of S8 with a centered frequency around 432.56 kHz after ALE-treating the SCD cantilever for 380 h. The resonance frequency spectra from other SCD cantilevers after the ALE in comparison with the same devices as released can be found in Fig. S3 (Supplemental Material [34]). The high crystal quality and crystal uniformity of the SCD cantilever were confirmed by a Raman spectrum with a narrow FWHM of 2.70 cm^{-1} with a deviation less than 0.3 cm^{-1} throughout the cantilever [Fig. 3(b)]. In addition, the peak position of the Raman spectra shows little shift, suggesting a small strain in the cantilever. The quality factor Q_{lor} can be calculated by fitting the resonance frequency spectra using the Lorentzian function. The typical relationships between the Q_{lor} values and the ALE treatment time were plotted in Fig. 3(c). An increase of the Q_{lor} was observed as the ALE duration is prolonged. Due to the frequency resolution limit or time comsumed in the frequency sweep (Fig. S4, Supplemental Material [34]), more accurate Q factors were deduced by the ring-down measurement. The time constant of the demodulator was set to be 1 ms, much less than the decay times of the cantilevers. Figure 3(d) shows the ring-down plots of cantilever S8 as released and after ALE of 380 h. The decay time of the cantilever increases markedly from 20 to 321 ms after ALE for 380 h. The Q factors were calculated by

$$Q = \pi\tau f_0, \tag{2}$$

where τ is a characteristic decay time of the cantilever. Table SI (Supplemental Material [34]) lists the resonance performance of 15 SCD cantilevers with different dimensions

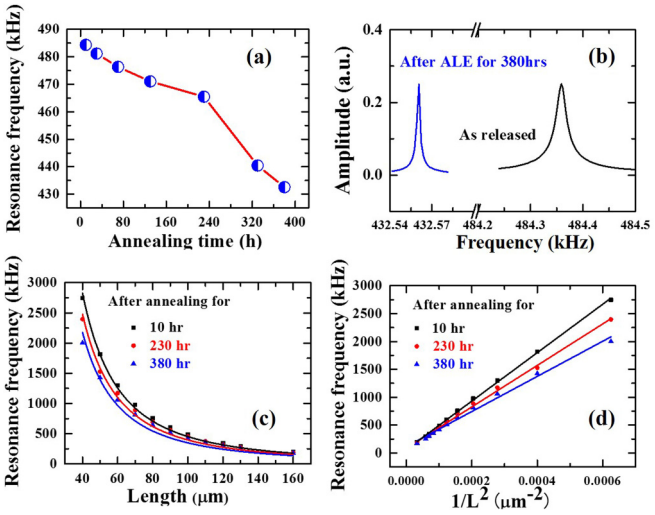

FIG. 4. (a) The relationship between resonance frequency and ALE duration for cantilever S8. (b) The resonance frequency shift of cantilever S8 after ALE treatment. (c) The dependence of resonance frequency on the cantilever length after ALE treating for 10, 230, and 380 h. (d) The linear fitting of the resonance frequency with $1/L^2$.

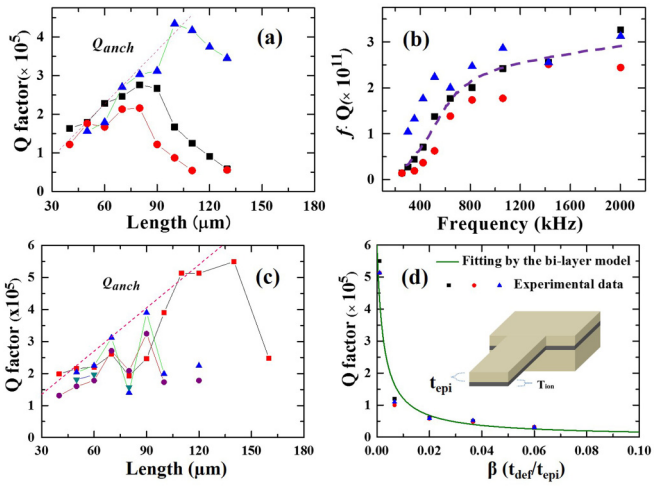

FIG. 5. (a) Dependence of Q factor on the cantilever length and (b) relationship between the product $f_0 Q$ and resonance frequency after 380-h ALE treatment. (c) Dependence of Q factor on the cantilever length after treatment by H_2 plasma. Dashed lines: theoretical anchor loss. The different symbols showing the cantilevers of each group at different locations. (b) Sketch of bilayer model and theoretical fitting curve. t_{def}: thickness of the mostly defective layer in the ion-implanted layer. T_{ion}: thickness of the ion-implanted SCD layer. For a certain length, several SCD cantilevers were measured.

after ALE for 380 h. The Q factors of the SCD cantilever are more than one order of magnitude higher than those of the as-released ones. The Q factor as high as 434 000 is obtained by the ring-down method, corresponding to a minimal force detectivity F_{th} as low as around 2.6×10^{-16} N/Hz$^{1/2}$. Table S1 (Supplemental Material [34]) reveals the Q factors ranging from 213 000 to 434 000, which presents a high reproducibility of the ALE method to fabricate high-Q-factor SCD cantilevers.

To investigate the effect of the ion-implantation induced defect in the SCD cantilever on the Q factor, the ALE was performed by several steps with a total duration from the initial 10 h to 30, 70, 130, 230, 330, and final 380 h. The resonance frequency and the Q factors were analyzed after each ALE step. In order to elucidate the dramatic improvement of the SCD resonator's Q factors, the variation of resonance frequencies with the ALE duration is plotted in Fig. 4(a). The ALE induces an obvious redshift of the resonance frequency from 484.358 kHz (after 10-h ALE) down to 432.560 kHz (after 380-h ALE) for cantilever S8, as displayed in Fig. 4(b). Such a frequency shift occurs for all the SCD cantilevers (Fig. S5, Supplemental Material [34]). Based on the frequency shift, the reduction of the SCD cantilever thickness can be calculated from Eq. (1), which was estimated to be about 180 nm after 380-h ALE. Therefore, the corresponding etching speed of the cantilever is estimated to be around ~0.5 nm/h (0.25 nm/h for one side). Considering that the ALE etches both the surface and the bottom of the SCD cantilevers, the etched thickness of the ion-damaged SCD layer is ~90 nm. This thickness is similar to that of the top-part diamond observed in Fig. 2(a). We note that, as shown in Fig. 3, the Q factors of the SCD cantilevers are markedly improved after ALE for 330 h and increase further after 380 h. The significant improvement of the Q factors is due to the etching of most of the defects by ion implantation at the bottom of the SCD cantilever. Note that the Q factor of the SCD cantilever is limited by the total number of defects induced by ion implantation. Therefore, one cannot expect the greatest increase in Q factor at the beginning of the ALE treatment for 10 h (~2.5-nm etched damaged layer from the bottom of the cantilever). The increase of Q factor with etched thickness is consistent with the damage profile by ion implantation observed by experiments and calculated by TRIM [36]. The edge wall was not so much modified by ALE treatment (Fig. S6, Supplemental Material [34]), excluding the edge etching effect on the marked improvement of the Q factor. Note that after the ALE for 380 h, the length-dependent resonance frequency still follows well the Euler-Bernoulli theory, as revealed in Figs. 4(c) and 4(d).

To further investigate the energy dissipation mechanism, the relationship between the Q factors and the cantilever length is examined, as shown in Fig. 5(a). The Q factor vs length reveals three regions: The Q factor increases nearly linearly with the cantilever length. When the cantilever length is larger than 100 μm, the Q factor starts to saturate, and finally decreases for longer cantilevers. On the other hand, with increasing the resonance frequency, the Q factor is deteriorated. As a consequence, it is considered a challenge to design a mechanical resonator with high Q factor and high f simultaneously, which can be quantified by the product of these two quantities fQ [37]. The variation of fQ vs f is shown in Fig. 5(b). In our case, the product of fQ shows nearly linear improvement with f, and reaches a maximum fQ equal to 3.26×10^{11} Hz with a high Q factor of 16.3×10^4 at 2.0029 MHz. Besides, a further step of H_2 plasma treatment was conducted after the 380-h ALE treatment. Figure 5(c) shows the Q factor vs cantilever length after H_2 plasma treating the ALE processed SCD cantilevers for 1 h at 800 °C.

The Q factor of 550 000 is achieved. Extending the H_2 plasma treatment for another 1 h further improved the Q factor to more than 710 000 for cantilever S9 and the maximum Q factor after this H_2 plasma treatment is 758 219. The Q factor reaches over 1 000 000 after another 2-h H_2 plasma treatment (Fig. S7, Supplemental Material [34]). The improvement of the Q factors by H_2 plasma treatment is due to further etching away of the defects. An additional 20-hALE treatment in an oxygen ambient at 500 °C was also performed. It was observed that the Q factors tended to be saturated (Fig. S8, Supplemental Material [34]).The Q factor is comparable to the highest value reported ever for a SCD cantilever fabricated by the DOI technique [11]. However, the fQ product in our case is more than one order of magnitude higher those of SCD cantilevers reported in Ref. [11]. The resulting force sensitivity is around $1.6 \times 10^{-16}\,\mathrm{N/Hz^{1/2}}$. The Q factors are one or more order of magnitude larger than those of the state-of-the-art cantilevers fabricated from polycrystalline diamond, single-crystal silicon, and other materials [7,18,19]. We compare the effect of different treatments on the Q factors of the SCD cantilevers: (1) ALE treatment for 380 h, (2) boiling in a mixture acid solution of $HNO_3 + H_2SO_4$, and (3) H_2 plasma treatment for 1h. The Q factors of the SCD cantilevers with different treatments are shown in Fig. S9 (Supplemental Material [34]). The wet treatment in the acid degraded the Q factor due to the enhancement of adhesion force. The ultrahigh Q factor is recovered after H_2 plasma treatment. We have investigated 27 SCD cantilevers (already ALE treated for 380 h) by H_2 plasma treatment and found that 24 of them had a redshift of the resonance frequency relative to the 380-h ALE-treated cantilevers due to the etching effect. We note that after the ALE treatment for 380 h, the surface was still very smooth with a RMS roughness around 0.4 nm (Fig. S10, Supplemental Material [34]). H_2 plasma has little effect on the surface morphology.

Generally, the overall Q factor depends on air damping, anchor loss Q_{anch}, bulk or surface loss (Q_{bulk} or O_{sur}), thermal elastic damping (Q_{TED}), and others. Here we discuss the mechanisms one by one. Air damping can be clearly excluded since the measurements were conducted in a vacuum. For a simple cantilever with flexural out-of-plane mode, the anchor loss limited Q factor can be expressed as [38]

$$Q_{\mathrm{anch}} = \alpha \frac{L}{w}, \tag{3}$$

where parameter α is a material-dependent experimental factor, which is proportional to $(t_b/t)^2$; t_b stands for the thickness of the base and t is the thickness of cantilever; w is the width of the cantilever. The clamping loss mechanism is accounted for both of the ALE-treated and H_2-plasma-treated SCD cantilevers with short length, with α as 30 000–36 000. This α value is reasonable considering that t_b is around 500 μm. Surface states can also strongly affect the Q factor, which is explained by a surface loss as

$$Q_{\mathrm{suf}} = \frac{wt}{2\delta(3w+t)} \frac{E_1}{E_2^S}, \tag{4}$$

where δ is the characteristic thickness of the "surface layer" and w stands for the width of the cantilever [8]. This loss limits the Q factors of the SCD cantilevers with long length [Figs. 5(a) and Fig. 5(c)] for each cantilever group plotted in different symbols). Note that the Q factor of a certain length SCD cantilever shows different values due to spatial inhomogeneity. The H_2 plasma treatment leads to H-terminated diamond surface, which differs from the oxygen annealing, or acid treatment induced O-terminated diamond surface [39,40]. Although O-terminated diamond surface is stable, a dry oxidation process of annealing in oxygen ambient is better than the wet method. The TED mechanism, the result of the transformation of elastic energy into thermal energy via thermal currents flowing between compressed and expanded regions of a deformed resonator [41,42], cannot explain the linear dependence of Q factor on length. It will be discussed later that the TED works at elevated temperatures.

The Q_{lor} factors of the SCD cantilevers before and after the ALE treatment up to 330 h were also investigated (Fig. S11, Supplemental Material [34]). Different from those cantilevers treated by the ALE for 380 h, the overall Q_{lor} factor shows little dependence on the length. This suggests that the defects limit the Q factor due to an insufficient reduction of the bottom damaged layer in the SCD cantilevers. We thus fit the Q factors by the bilayer model [35],

$$\frac{1}{Q} = \frac{1}{1+\beta}\left(\frac{1}{Q_{\mathrm{epi}}} + \beta \frac{1}{Q_{\mathrm{def}}}\right), \tag{5}$$

where Q_{epi} is the quality factor of epilayer diamond alone and Q_{def} represents the quality factor of the most defective layer by ion implantation at the bottom of the cantilever. The factor β is determined by

$$\beta = \frac{E_{\mathrm{def}} t_{\mathrm{def}}}{E_{\mathrm{epi}} t_{\mathrm{epi}}}, \tag{6}$$

where E_{def} and E_{epi} are assumed to be equal and then β is simplified to $t_{\mathrm{def}}/t_{\mathrm{epi}}$, the ratio of ion-damaged layer thickness and epilayer. The fitted curve from this equation is plotted in Fig. 5(d), where Q_{epi} is substituted by 1 000 000 and Q_{def} is set to be 1000, respectively. With β close to 0, which corresponds to the elimination of the mostly defective layer, the Q factors show abrupt improvement. Therefore, the bulk loss by the defective layer dominates the energy loss for both the as-fabricated SCD cantilevers and the cantilevers with insufficient ALE treatment.

IV. CONCLUSIONS

In summary, we demonstrated SCD-on-SCD mechanical cantilever-type resonators with ultrahigh Q factors over 1 000 000 by using a smart-cut method and atomic scale etching within 1-nm accuracy. One significant advance or feature of the present concept is the capability for the monolithic integration of SCD MEMS/NEMS with SCD electronics and quantum centers [31]. This work opens the avenue to develop the next-generation integrated MEMS/NEMS and optomechanical systems with markedly boosted performance and reliability for ultrasensitive sensing, low-loss rf signal processing, scanned microprobes, and quantum sciences.

ACKNOWLEDGMENTS

This work was supported by JSPS KAKENHI (Grants No. 15H03999 and No. 26220903), TIA, and Nanotechnology Platform, MEXT, Japan. H.W., T.L., and J.Y. were supported by Science Challenge Project (Grant No. TZ 2017003) and the National Key Research Development Program of China (Grants No. 2016YFA0301200 and No. 2014CB848700),

[1] D. Maja, W. Marcel, C. H. Schwalb, J. D. Adams, S. Vladimir, H. Michael, and G. E. Fantner, Nat. Commun. **7**, 12487 (2016).
[2] A. Ramezany, M. Mahdavi, and S. Pourkamali, Microsyst. Nanoeng. **2**, 16004 (2016).
[3] J. Teissier, A. Barfuss, P. Appel, E. Neu, and P. Maletinsky, Phys. Rev. Lett. **113**, 020503 (2014).
[4] S. Meesala, Y.-I. Sohn, H. A. Atikian, S. Kim, M. J. Burek, J. T. Choy, and M. Lončar, Phys. Rev. Appl. **5**, 034010 (2016).
[5] P. Ovartchaiyapong, K. W. Lee, B. A. Myers, and A. C. B. Jayich, Nat. Commun. **5**, 4429 (2014).
[6] R. Abdolvand, B. Bahreyni, J. E.-Y. Lee, and F. Nabki, Micromachines **7**, 160 (2016).
[7] M. Kanik, P. Bordeenithikasem, G. Kumar, E. Kinser, and J. Schroers, Appl. Phys. Lett. **105**, 131911 (2014).
[8] K. Y. Yasumura, T. D. Stowe, E. M. Chow, T. Pfafman, T. W. Kenny, B. C. Stipe, and D. Rugar, J. Microelectromech. Syst. **9**, 117 (2000).
[9] M. Liao, T. Masaya, L. W. Sang, T. Tokuyuki, I. Masataka, and K. Yasuo, Jpn. J. Appl. Phys. **56**, 024101 (2017).
[10] P. Ovartchaiyapong, L. M. A. Pascal, B. A. Myers, P. Lauria, and A. C. B. Jayich, Appl. Phys. Lett. **101**, 163505 (2012).
[11] Y. Tao, J. M. Boss, B. A. Moores, and C. L. Degen, Nat. Commun. **5**, 3638 (2014).
[12] M. Liao, M. Toda, L. Sang, S. Hishita, S. Tanaka, and Y. Koide, Appl. Phys. Lett. **105**, 251904 (2014).
[13] A. V. Sumant, O. Auciello, R. W. Carpick, S. Srinivasan, and J. E. Butler, MRS Bull. **35**, 281 (2010).
[14] M. Nesladek, D. Tromson, C. Mer, P. Bergonzo, P. Hubik, and J. J. Mares, Appl. Phys. Lett. **88**, 232111 (2006).
[15] H. Najar, C. Yang, A. Heidari, L. W. Lin, and D. A. Horsley, J. Microelectromech. Syst. **24**, 2152 (2015).
[16] E. Sillero, O. A. Williams, V. Lebedev, V. Cimalla, C. C. Rohlig, C. E. Nebel, and F. Calle, J. Micromech. Microeng. **19**, 115016 (2009).
[17] A. Gaidarzhy, M. Imboden, P. Mohanty, J. Rankin, and B. W. Sheldon, Appl. Phys. Lett. **91**, 203503 (2007).
[18] N. Sepulveda, J. Lu, D. M. Aslam, and J. P. Sullivan, J. Microelectromech. Syst. **17**, 473 (2008).
[19] N. R. Parikh, J. D. Hunn, E. McGucken, M. L. Swanson, C. W. White, R. A. Rudder, D. Malta, J. B. Posthill, and R. J. Markunas, Appl. Phys. Lett. **61**, 3124 (1992).
[20] M. Poot and H. S. J. van der Zant, Phys. Rep. **511**, 273 (2012).
[21] P. Olivero, S. Rubanov, P. Reichart, B. C. Gibson, S. T. Huntington, J. Rabeau, A. D. Greentree, J. Salzman, D. Moore, D. N. Jamieson, and S. Prawer, Adv. Mater. **17**, 2427 (2005).
[22] I. Aharonovich, J. C. Lee, A. P. Magyar, B. B. Buckley, C. G. Yale, D. D. Awschalom, and E. L. Hu, Adv. Mater. **24**, OP54 (2012).
[23] A. H. Piracha, K. Ganesan, D. W. Lau, A. Stacey, L. P. Mcguinness, S. Tomljenovichanic, and S. Prawer, Nanoscale **8**, 6860 (2016).
[24] M. Liao, C. Li, S. Hishita, and Y. Koide, J. Micromech. Microeng. **20**, 085002 (2010).
[25] M. Liao, S. Hishita, E. Watanabe, S. Koizumi, and Y. Koide, Adv. Mater. **22**, 5393 (2010).
[26] H. Miyatake, K. Arima, O. Maida, T. Teraji, and T. Ito, Diamond Relat. Mater. **16**, 679 (2007).
[27] T. Tsuno, T. Tomikawa, S. I. Shikata, T. Imai, and N. Fujimori, Appl. Phys. Lett. **64**, 572 (1994).
[28] O. Maida, H. Miyatake, T. Teraji, and T. Ito, Diamond Relat. Mater. **17**, 435 (2008).
[29] H. Yamada, A. Chayahara, Y. Mokuno, N. Tsubouchi, and S. I. Shikata, Diamond Relat. Mater. **33**, 27 (2013).
[30] T. Teraji, J. Appl. Phys. **118**, 115304 (2015).
[31] T. Teraji, T. Yamamoto, K. Watanabe, Y. Koide, J. Isoya, S. Onoda, T. Ohshima, L. J. Rogers, F. Jelezko, and P. Neumann, Phys. Status Solidi **212**, 2365 (2015).
[32] H. Kawarada, H. Tsuboi, T. Naruo, and T. Yamada, Appl. Phys. Lett. **105**, 013510 (2014).
[33] M. K. Zalalutdinov, M. P. Ray, D. M. Photiadis, J. T. Robinson, J. W. Baldwin, J. E. Butler, T. I. Feygelson, B. B. Pate, and B. H. Houston, Nano Lett. **11**, 4304 (2011).
[34] See Supplemental Material at http://link.aps.org/supplemental/10.1103/PhysRevMaterials.2.090601 for length-dependent resonance frequency, frequency spectra, resonance frequency shift with ALE, morphology of the SCD walls, Q factors as treatment duration, surface treatment effect on Q factor, surface morphology of the SCD before and after ALE treatment, Q factors vs ALE duration, and Q factors after ALE for 380 h.
[35] M. J. Seitner, K. Gajo, and E. M. Weig, Appl. Phys. Lett. **105**, 213101 (2014).
[36] A. Uedono, T. Kawano, S. Tanigawa, R. Suzuki, T. Odaira, T. Mikado, S. Fuji, and S. Shikata, Jpn. J. Appl. Phys. **34**, 1772 (1995).
[37] C. M. Lin, Y. Y. Chen, V. V. Felmetsger, D. G. Senesky, and A. P. Pisano, Adv. Mater. **24**, 2722 (2012).
[38] M. Imboden and P. Mohanty, Phys. Rep. **534**, 89 (2014).
[39] S. J. Sque and R. Jones, Phys. Rev. B. **73**, 085313 (2006).
[40] Y. Kaibara, K. Sugata, M. Tachiki, H. Umezawa, and H. Kawarada, Diamond. Relat. Mater. **12**, 560 (2003).
[41] C. Zener, Phys. Rev. **53**, 90 (1938).
[42] R. Lifshitz and M. L. Roukes, Phys. Rev. B. **61**, 5600 (2000).